Published in final edited form as:

Environ Sci Technol. 2016 August 02; 50(15): 7982–7990. doi:10.1021/acs.est.6b01473.

Measured Wavelength-Dependent Absorption Enhancement of Internally Mixed Black Carbon with Absorbing and Non-absorbing Materials

Rian You[†,‡], **James G. Radney**[†], **Michael R. Zachariah**[†,‡], and **Christopher D. Zangmeister**[†,*]

[†]Material Measurement Laboratory, National Institute of Standards and Technology, Gaithersburg, Maryland 20899

[‡]Department of Chemistry and Biochemistry, University of Maryland, College Park, Maryland 20742

Abstract

Optical absorption spectra of laboratory generated aerosols consisting of black carbon (BC) internally mixed with non-absorbing materials (ammonium sulfate, AS, and sodium chloride, NaCl) and BC with a weakly absorbing brown carbon surrogate derived from humic acid (HA) were measured across the visible to near-IR (550 nm to 840 nm). Spectra were measured *in-situ* using a photoacoustic spectrometer and step-scanning a supercontinuum laser source with a tunable wavelength and bandwidth filter. BC had a mass-specific absorption cross section (*MAC*) of 7.89 ± 0.25 $m^2\ g^{-1}$ at λ = 550 nm and an absorption Ångström exponent (*AAE*) of 1.03 ± 0.09 (2σ). For internally mixed BC, the ratio of BC mass to the total mass of the mixture was chosen as 0.13 to mimic particles observed in the terrestrial atmosphere. The manner in which BC mixed with each material was determined from transmission electron microscopy (TEM). AS/BC and HA/BC particles were fully internally mixed and the BC was both internally and externally mixed for NaCl/BC particles. The AS/BC, NaCl/BC and HA/BC particles had *AAE*s of 1.43 ± 0.05, 1.34 ± 0.06 and 1.91 ± 0.05, respectively. The observed absorption enhancement of mixed BC relative to the pure BC was wavelength dependent for AS/BC and decreased from 1.5 at λ = 550 nm with increasing wavelength while the NaCl/BC enhancement was essentially wavelength independent. For HA/BC, the enhancement ranged from 2 to 3 and was strongly wavelength dependent. Removal of the HA absorption contribution to enhancement revealed that the enhancement was ≈ 1.5 and independent of wavelength.

Graphical Abstract

*Corresponding Author: cdzang@nist.gov. Phone: (301)975-8709. Fax: (301)975-3670.

Author Contributions

The manuscript was written through contributions of all authors. All authors have given approval of the final version of the manuscript.

The authors declare no competing financial interests.

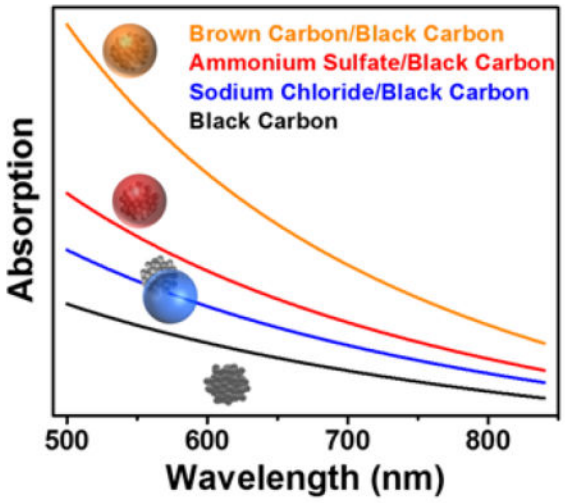

INTRODUCTION

Black carbon (BC) is produced from the incomplete combustion of biomass and fossil fuels, and consists of layered graphitic carbon monomers 20 nm to 40 nm in diameter[1] that are aggregated into more complex structures that strongly absorb light across the visible spectrum.[2] It has been estimated that BC is the second largest contributor to global warming after CO_2.[3] BC aggregates are often internally and/or externally mixed with other species (sulfate, nitrates, carbonaceous organics, etc.).[4–12] The resulting particle morphology, referred to here as the mixing state, can have BC surface bound, or partially- or fully-embedded (engulfed) with BC either centrally (concentric) or off-centrally (eccentric) located within the particle.[8,13]

Changes to the per particle absorption strength (i.e. absorption cross section) and spectral shape when other atmospheric components coat, embed in or mix with BC have drawn significant attention[14–17] as absorption is typically enhanced beyond the bare particle case. Consistent with previous investigations,[17,20,22] we define the wavelength dependent absorption enhancement factor ($E_{Abs,\lambda}$) as the ratio of the absorption cross section (C_{Abs}) of the embedded particle ($C_{Abs,embed\ BC,\lambda}$) to that of the bare BC particle ($C_{Abs,BC,\lambda}$)

$$E_{Abs,\lambda} = \frac{C_{Abs,embed\ BC,\lambda}}{C_{Abs,BC,\lambda}} \quad (1)$$

where C_{Abs} is defined as

$$C_{Abs} = \frac{\alpha_{Abs}}{N} \quad (2)$$

and N is the number concentration of particles. The quantity α_{Abs} represents the absorption coefficient and is the fractional loss in light intensity due to absorption per unit propagation distance.

Considering the size of particles and the thickness of embedding material relevant in the atmosphere (i.e. comparable to or smaller than the wavelength of light), absorption enhancement arises from the gradual step-wise refractive index change between the medium (air), embedding material and the absorbing material (BC in most cases); i.e. the embedding material facilitates improved refractive index matching between the medium and absorbing material thereby behaving similar to an antireflective coating.[18] The observed enhancement is strongly dependent upon the size and absorption strength of the absorbing material, embedding thickness and embedding material. Previous investigations have referred to this refractive index matching as lensing whereby the embedding material focuses light towards the absorbing core.[17,19,20] We note that while lensing may be an appropriate descriptor in the geometric optics regime (particles much larger than the wavelength of light) it is not appropriate to use at these sizes.

For an absorbing core comprised of 10 nm aggregates embedded in a 1 μm non-absorbing shell the $E_{Abs,\lambda}$ can be greater than 10. However, for atmospherically relevant particles, the $E_{Abs,\lambda}$ is more modest and ranges between 1.5 and 1.9 for particles with shell diameters that are less than 1.6 times larger than the core diameter.[14] Ambient measurements show that the $E_{Abs,\lambda}$ of BC can be up to 2.4.[11,21–26] The discrepancy between field measurements and theoretical calculations of internally mixed, embedded particles can be computationally reduced with the consideration of an eccentrically-located single BC core in an internally mixed embedded particle or by the application of discrete dipole approximation method (DDA) or multiple sphere T-matrix method (MSTM) to account for the complex aggregate morphology and the interaction between spherules.[27–29] Moreover, it has been shown computationally that the mixing state of BC has a great impact on the absorption enhancement factor.[30] In contrast to the ambient field-based observations, laboratory measurements tend to coincide more closely to $E_{Abs,\lambda}$ predicted by the concentric sphere model.[2,31–33] Previous laboratory studies have concentrated on BC embedded in materials generated from the ozonolysis products from α-pinene,[34] glycerol and oleic acid,[32] and dioctyl sebacate,[21] and can produce a BC core embedded in an organic shell (core-shell model). These investigations observed that the core-shell model can be adequately captured from current theory, but are limited in relevance to particles observed in many field studies.[35] Further, in ambient studies the embedding material must be physically removed to measure the absorption by the BC core. Removal of the embedding material is typically done by volatilization, although the efficacy of removal remains questionable.[25,36] To our knowledge, however, no laboratory study has been reported on the absorption enhancement of heterogeneous BC particles with different mixing states in a controlled manner.

In addition to $E_{Abs,\lambda}$, spectral shape can be affected by particle mixing state. The absorption spectral dependence is commonly described by the absorption Ångström exponent (AAE)

$$C_{Abs,\lambda} = C_{Abs,0} \left(\frac{\lambda}{\lambda_0}\right)^{-AAE} \quad (3)$$

where $C_{Abs,\lambda}$ is the absorption cross section at wavelength λ. The terms $C_{Abs,0}$, and λ_0 have been included as the values for a reference wavelength; presently, λ_0 = 550 nm for comparison to prior work. The AAE for BC is typically quoted as being near unity and assumes a wavelength independent refractive index for particles < 40 nm in diameter.[37] Recent modeling has shown that BC cores embedded within a non-absorbing matrix (50 nm embedding in a 300 nm BC core) can increase the AAE from an initial value of 1.3 up to 1.6.[17] BC can also be mixed or embedded with weakly absorbing carbonaceous materials derived from combustion of biomass and biofuels, termed brown carbon (BrC). BrC is typically quoted as having AAE values ranging from 1.5 to ≈ 7.0.[24,31,38–45] Additional experimental studies are required to fully understand the impact of BC embedded within BrC.

Direct *in-situ* absorption measurements can be made using a photoacoustic spectrometer. Ideally, absorption measurements at many points spanning the visible portion of the spectral window would be collected to elucidate the wavelength dependence of embedded BC. In practice, four or fewer wavelengths are typically used as a sufficiently intense source (e.g. laser) is necessary to generate a measurable acoustic signal; further, the use of multiple sources may require the use of multiple acoustic resonators and data acquisition systems. It is possible to equip a photoacoustic spectrometer with a broad-band source such as an optical parametrical oscillator,[46] a Hg arc lamp[47] or supercontinuum laser[48,49] to acquire step-scanned absorption spectra. In the present study 7 points were used to comprise a spectrum, although only two wavelengths are required to fit Eq. 3, where it will reduce to the explicit form used extensively in prior studies.[50–53]

The discrepancy between ambient field-based measurements and computational-based predictions of absorption for spherical systems of BC in different mixing states requires measurements of well-characterized laboratory-based aerosol. This investigation describes absorption measurements of BC mixed with non-absorbing materials (ammonium sulfate and sodium chloride) and a weakly absorbing BrC surrogate, humic acid (HA); all of which are atmospherically relevant species. The mass mixing ratio (χ_{BC}) defined as the ratio of BC mass to the mass of the total mixture, was chosen as 0.13, similar to particles collected in the terrestrial atmosphere.[13] The absorption spectra were measured using a photoacoustic spectrometer coupled to a supercontinuum light source with a tunable wavelength and bandwidth filter. The measured data as a function of embedding material and mixing state were compared to E_{Abs} calculated using the T-matrix method.

MATERIALS & METHODS

A schematic of the experimental setup used is shown in Figure 1. Aerosols were generated and conditioned before being passed to a differential mobility analyzer (DMA) and an aerosol particle mass analyzer (APM) to select the mobility diameter (D_p) and mass (m_p), respectively. Optical absorption was measured by a photoacoustic spectrometer (PA) that

utilizes a supercontinuum laser as its light source. A condensation particle counter (CPC) was situated downstream to measure aerosol number density. Using both mobility and mass selection facilitates isolation and selection of particles bearing a +1 charge. Care was used to ensure that only +1 particles were selected by measuring particle extinction as function of m_p as previously described in Radney and Zangmeister (2016).[54]

Aerosol Generation and Morphological Characterization

BC was generated from Cab-O-Jet 200 (Cabot Corp., 20.03 weight percent solids), a material generated from the combustion of organic fuel stock.[55] This material was chosen for its water solubility and its spectroscopic and morphological similarities to aged BC (see discussions in Results section). Cab-O-Jet in solution consists of dispersed monomers ≈ 30 nm in diameter as evidenced by transmission electron microscopy (TEM) images (see Supporting Information Fig. S1). Atomization of a Cab-O-Jet solution produces water droplets containing multiple monomers. Upon drying, the monomers combine and collapse into a structure that appears similar to collapsed BC observed in the terrestrial atmosphere.[56,57]

A BrC surrogate (AAE > 4) consisting of humic acids (HA) was prepared from Ful-Humix (Faust BioAg Inc., 50 weight percent humic acids) by dissolving 500 mg in 15 mL of DI H_2O. The solution was centrifuged for 30 min, the supernatant was decanted and collected, and centrifuged for an additional 30 min. The supernatant was again collected, combined and subsequently filtered to remove any residual solids. The filtered solution was then air dried. The density of the HA was measured in bulk (mass per unit volume) and calculated as the average effective density from the mass-mobility scaling relationship (see discussion in Results section and Supporting Information). From the residual dried solid material, a stock solution of 5 mg mL^{-1} was prepared for absorption measurements. The non-absorbing materials, ammonium sulfate (AS, Sigma Aldrich) and sodium chloride (NaCl, Sigma Aldrich) were used as-received and stock solutions of 5 mg mL^{-1} were prepared.

To mimic BC containing aerosol measured in Mexico City aerosol plumes,[13] internally mixed particles were produced by co-atomization of a single aqueous solution containing both BC and either AS, NaCl or HA at a 0.13 BC mass fraction (χ_{BC}) in a liquid jet cross flow atomizer (TSI 3076, 30 psig); BC volume fractions were 0.12, 0.15 and 0.11 for the AS/BC, NaCl/BC and HA/BC particles, respectively. At this pressure, ≈ 2.2 L min^{-1} of flow is generated by the atomizer of which ≈ 0.5 L min^{-1} was sampled and the remainder exhausted into a laboratory exhaust. Both Cab-O-Jet (BC) and HA required extensive drying due to their hygroscopic nature and extra effort was made to remove particle-bound water in order to avoid additional absorption enhancement[48] or potential photoacoustic response dampening[58–61] from water adsorption. After atomization, aerosols were passed through two SiO_2 desiccation dryers (TSI 3062) and a Nafion drying tube (PermaPure MD-700-48F-3) with the counter flow relative humidity (RH) held at < 5 %. After drying, particles were size selected by a DMA (TSI 3082) using 5 L min^{-1} sheath flow and 0.5 L min^{-1} aerosol flow. The particles were then mass-selected using an APM as described previously.[48]

For TEM measurements particles were collected using an electrostatic aerosol precipitator (TSI 3089) on TEM grids (200-mesh copper grids embedded with lacey carbon film) at −9.3

kV collection voltage. The morphology and mixing states of the BC particles were imaged using a JEOL 2100 TEM at an accelerating voltage of 200 kV.

Optical Measurements

Aerosol optical absorption spectra were measured using a PA spectrometer as described in Radney and Zangmeister (2015),[48] which can operate across a range spanning from visible to near IR (λ = 550 nm to 840 nm) using a supercontinuum laser (NKT Photonics SuperK Extreme EXR-15) and tunable wavelength and bandpass filter (NKT Photonics SuperK Varia). The particles were illuminated by an intensity modulated laser (via a mechanical chopper) at the resonant frequency of the acoustic cavity (≈ 1640 Hz at 296 K in ambient air).[62] Absorbed optical energy is thermally re-emitted generating a standing pressure wave (i.e. sound wave) at the modulation frequency that was measured by a calibrated microphone located at the resonator antinode, as described previously.[48] A lock-in amplifier (Stanford Research Systems, SR830) was employed for phase-sensitive detection allowing for the absorption coefficients to be calculated from

$$\alpha_{Abs} = \frac{\sqrt{(x-x_0)^2+(y-y_0)^2}}{C_c \beta_m W_{pp}} \quad (5)$$

where x, y, C_c, β_m and W_{pp} are the in-phase and quadrature signals measured by the lock-in amplifier, the acoustic cell constant, the microphone responsivity and the peak-to-peak laser power, respectively. For the current system $C_c\beta_m$ is 0.187 V m W^{-1}. The terms x_0 and y_0 have been included to account for the lock-in amplifier's small, but non-zero background signal measured when the laser is off.

Modeling BC Optical Properties

The optical properties of bare BC and BC mixed with other components were modeled using the multiple-sphere superposition T-matrix method.[63] BC aggregates were constructed using a diffusion-limited aggregation algorithm[64] as described in Supporting Information. Calculated absorption of BC mixed with other species (i.e. AS, NaCl & BrC) assumed BC possessed a similar morphology to bare BC, except that the number of monomers was scaled relative to the mass ratio (0.13 mass ratio). Two cases were investigated, fully- and partially-embedded where either: 1) a single host sphere was used with the diameter identical to the D_p selected by the DMA, with the BC aggregate's center of mass overlapping that of the host sphere, or 2) half of the monomers in the BC aggregate were moved radially to the outside of the sphere and remained attached, respectively.

RESULTS

Characterization of Bare BC

Bare BC aerosol had a compact, spherical morphology comprised of 30 nm monomers. TEM images revealed monomers with discontinuous onion-like fringes, consistent with flame generated soot and indistinguishable from TEM images of aged soot in the

atmosphere,[1] see Fig. 2a. The measured mass-mobility scaling exponent D_{fm} was 2.83 ± 0.01 consistent with the nearly spherical shape observed in TEM images. The effective density ρ_{eff}, defined as

$$\rho_{eff} = \frac{6m_p}{\pi D_p^3} \quad (6)$$

was measured as (0.78 ± 0.05) g cm^{-3} over a D_p range between 100 nm and 300 nm. Figure 2b shows the measured C_{Abs} at λ = 600 nm, 700 nm and 800 nm of bare BC as a function of particle mass spanning from 0.47 fg to 10.48 fg; D_p = 100 nm to 300 nm in 50 nm increments. The linearity at each wavelength indicates that the C_{Abs} scales with particle mass (i.e. Rayleigh regime) across the spectral region used in this investigation up to the pure 10.48 fg BC particle. For comparison, the average internally mixed AS/BC and NaCl/BC particles (see below) contained ≈ 1.4 fg and 1.7 fg of BC, respectively. Due to the wide mass range over which C_{Abs} is linear for pure BC particles, we expect the BC portion of the internally mixed particles to behave similarly.

A better resolved absorption spectrum ($\Delta\lambda$ = 50 nm) for BC particles with a 250 nm mobility diameter corresponding to a BC mass of 6.3 fg is shown in Fig. 2c. Here the data has been plotted as C_{Abs} versus wavelength, instead of C_{Abs} versus mass as in Fig. 2b, as absorption depends only upon mass for all measured wavelengths (i.e. linearity of traces in Fig. 2b).[65] The MAC (defined as C_{Abs}/m_p) at 550 nm is (7.89 ± 0.25) m^2 g^{-1} and the AAE is 1.03 ± 0.09 over the measured wavelength range, similar to the average MAC and AAE for BC reported in prior studies (all reported uncertainties are 2σ).[19,66]

The RI at 660 nm of bare BC was calculated as (1.77 ± 0.02) + (0.80 ± 0.02)i, see discussion in Supporting Information. A broad range of RIs for atmospheric BC are documented in the literature.[67–69] The RI of the bare BC measured in this study is at the upper end of the previously published RI values for atmospheric BC, but similar to other investigations for particles with compact morphology.[19,68] To validate the BC parameters used in subsequent calculations, the absorption spectrum of bare BC was calculated using the T-matrix method[29] using a refractive index of m = 1.77 + 0.80i and an aggregate structure calculated using DLCA with k_0 = 1.2, D_f = 2.83, N_m = 218 and using the calculated BC RI (see Supporting Information). The BC RI was assumed to be wavelength independent as discussed in Bond and Bergstrom (2006).[19] Using these assumptions, the T-matrix is able to adequately capture the measured C_{Abs} and AAE, see solid red line in Fig. 2c.

Characterization of Embedded BC Mixing State

The absorption spectrum of BC embedded in three atmospherically relevant materials was measured for two non-absorbing materials (AS and NaCl) and a surrogate for brown carbon, HA (i.e. Ångström exponent ≥ 4).[17] BC particles can be embedded with AS and/or other aerosol at a BC mass fraction (χ_{BC}) ≈ 0.1.[13] Particle mixing state and optical properties are influenced by the interaction between BC and the embedding material,[13] drying rate[22] and history.[70]

In the present investigation, TEM images show structural differences for AS/BC, NaCl/BC and HA/BC, see Fig. 3, for 250 nm mobility diameter particles. AS/BC and HA/BC formed spherical particles with BC aggregates fully embedded within an AS or HA shell (Fig. 3a and 3c, respectively). NaCl/BC particles have a cubic NaCl shell with BC aggregates protruding from the particle interior to its periphery (Fig. 3b). Further evidence of the particle mixing state was determined by utilizing the electron beam from the TEM to melt and desorb the embedding material and reveal the particle interior, showing the presence of BC aggregates (see Supporting Information Figure S6 for images showing time series of embedding material melting). For NaCl/BC, aggregates were observed both internal and external to the embedding material.

Absorption of BC Embedded in Non-absorbing Materials

Below we focus on how mixing state influences particle absorption. We first concentrate on the optical properties of BC mixed with non-absorbing materials. Figure 4a shows the measured C_{Abs} spectra spanning between λ = 550 nm and 840 nm for particles that were size and mass selected at D_p = 250 nm and m_p = (13.50 ± 0.06) fg and (11.48 ± 0.06) fg for AS and NaCl, respectively with χ_{BC} = 0.13. The absorption cross section is higher for the fully embedded in AS versus the partially embedded NaCl. The spectra of the embedded particles have higher *AAE*s than bare BC; 1.43 ± 0.05 for AS/BC and 1.34 ± 0.06 for NaCl/BC versus 1.03 ± 0.09 for bare BC. The absorption enhancement of embedded BC (E_{Abs}) is based on Eq. 1 with C_{Abs} of the BC core calculated from the particle mass, BC mass fraction and *MAC* of 250 nm particles:

$$E_{Abs,\lambda} = \frac{C_{Abs,embed\ BC,\lambda}}{m_p\ \chi_{BC}\ MAC_{BC,\lambda}} \quad (7)$$

At the shortest wavelengths, E_{Abs} is within 2σ for both the AS/BC and NaCl/BC systems. Towards the long-wave side of the spectrum, E_{Abs} values for both systems differ as NaCl/BC has remained nearly constant and AS/BC has decreased.

Wavelength dependent E_{Abs} have been calculated previously for embedded BC using spherical particle Mie theory,[17] but to our knowledge the AS/BC data represent the first measured spectra showing a wavelength dependent E_{Abs} for embedded BC; the NaCl/BC E_{Abs} is wavelength independent across the measured spectral range. We used the T-matrix method to investigate if the method is able to capture the measured spectral dependence for each embedding material. Calculations were run for fully-embedded and half-embedded BC. The simulated enhancement spectra are shown in Fig. 4a for each case where the lower (dashed) and upper (solid) bounds represent the half-embedded and the fully-embedded cases, respectively. The region in between these two values represents mixing states migrating from half-embedded to fully- embedded BC, and assumes the BC aggregate's center of mass overlaps that of the host sphere. Moving BC aggregates off center results in less than 3% decrease in absorption cross section, consistent with previous calculations.[26] The corresponding simulated and measured *AAE*s are shown in Table 1.

Absorption of BC with Absorbing Material

A weakly absorbing BrC surrogate material was isolated from humic acid extracts as described in the Materials & Methods. Upon atomization and drying, pure HA forms spherical particles with an average effective density of (1.5 ± 0.1) g cm^{-3}, as determined from the mass-mobility scaling relationship (D_{fm} = 3.10 ± 0.04). The RI of HA was determined to be (1.58 ± 0.01) + (0.02 ± 0.01)*i* at λ = 660 nm. For T-matrix calculations, we assumed the real component of RI was invariant with wavelength and the imaginary part of the RI is well described by the absorption spectrum of the material in aqueous solution (see Supporting Information for HA refractive index determination and aqueous absorption spectrum). The absorption spectrum of HA aerosol is shown in Fig. 5a, and exhibits an AAE of 5.31 ± 0.14. The MAC of HA aerosol was (0.85 ± 0.06) m^2 g^{-1} at 550 nm, nearly an order of magnitude lower than that of BC at the same wavelength, and is comparable to strongly absorbing BrC in prior work.[71]

At a χ_{BC} = 0.13, C_{Abs} increases by a factor of 2 to 3 relative to the pure HA at the same mobility diameter. The AAE of BC embedded in HA is 1.91 ± 0.05, lower than that of pure HA but higher than that of BC embedded in AS or NaCl. For modeling we adopted a single sphere model for the pure HA and a fully-embedded model for HA/BC particles, consistent with TEM images of BC embedded in HA. The T-matrix calculated C_{Abs} spectrum agrees well with the experimental results in each case, as shown by the solid lines in Fig. 5a.

The $E_{Abs,\lambda}$ of BC embedded in HA was calculated using two methods. Using Eq. 1, $E_{Abs,\lambda}$ includes the impact of HA absorption and enhancement of BC absorption. For the second method, the inherent relative contributions to absorption from HA is removed by redefining $E_{Abs,\lambda}$ as

$$E_{Abs-HA,\lambda}=\frac{C_{Abs,embed\ BC,\lambda}}{(1-\chi_{BC})\ m_p\ MAC_{HA,\lambda}+\chi_{BC}\ m_p\ MAC_{BC,\lambda}} \quad (8)$$

where $MAC_{HA,\lambda}$ represents the MAC of the pure HA. Note that $E_{Abs\text{-}HA,\lambda}$ when applied to BC embedded in HA, describes the E_{Abs} arising only from BC absorption enhancement and reduces to Eq. 7 when applied to the non-absorbing material. Both results are shown in Figure 5b. The $E_{Abs,\lambda}$ shows an increase up to a factor of 3 at the shortest measured wavelengths and is 1.6 in the near-IR. Removing HA absorption from $E_{Abs,\lambda}$ shows that much of the enhancement at short wavelengths is a result of HA absorption as seen by the relatively constant $E_{Abs\text{-}HA,\lambda}$ in Fig. 5b. This trend was first predicted in prior calculations using spherical particle Mie theory, where the data are similar in shape and magnitude to 300 nm absorbing core with a weakly absorbing 100 nm thick embedding.[17]

DISCUSSION

In this investigation the mass mixing ratio and mobility diameter of internally mixed BC and NaCl, AS or HA particles were held constant at χ_{BC} = 0.13 and 250 nm, respectively. The primary variables that differ between the embedding materials are density, refractive index and how each material interacts with BC under the conditions of aerosol generation to form

particles (mixing state). Below we highlight how each variable impacts $E_{Abs,\lambda}$ using the simplest case of spherical particles. Due to density differences between the embedding materials, the χ_{BC} corresponds to a 133 nm, 127 nm and 120 nm BC core embedded in NaCl, AS and HA, respectively. Using a core-shell model in conjunction with Mie theory to calculate $E_{Abs,\lambda}$ for each of the non-absorbing core/shell diameters results in an $E_{Abs,\lambda}$ that is 4% ± 1% higher for NaCl/BC than AS/BC over the 550 nm and 850 nm wavelength range studied here (see Supporting Information Figure S7). The refractive index of the coating material also affects the calculated $E_{Abs,\lambda}$. This is best shown by keeping the BC core diameter constant (127 nm) and varying the coating refractive index, where $E_{abs,\lambda}$ increases an additional 0.5% to 1% for NaCl/BC over AS/BC. Thus, for equivalent 250 nm particles using an idealized spherical core-shell model, the $E_{Abs,\lambda}$ for NaCl/BC is calculated to be 5% to 6% higher than AS/BC. TEM images show that for NaCl/BC BC is partially embedded in NaCl, whereas BC is fully embedded by AS. Despite these differences, the measured $E_{Abs,\lambda}$ are equivalent at the shortest measured wavelength region and is up to 15% higher in the near-IR for NaCl/BC, suggesting that using simple core-shell spherical models do not adequately capture $E_{Abs,\lambda}$ for embedded particles.

The spectral shape and wavelength dependence of C_{Abs} can also be described by the measured AAE when compared to pure BC. The AAE for NaCl/BC and AS/BC are within the 2σ measurement uncertainty, see Table 1, indicating that for BC mixed with non-absorbing materials the AAE is near 1.4 and independent of particle mixing state. For HA/BC the AAE is nearly 2. Prior modelling studies of BC embedded in absorbing and non-absorbing materials have classified the AAE into two regimes to help better describe measured ambient aerosol, where BC embedded with non-absorbing materials have an $AAE < 1.6$, whereas only BC embedded with an absorbing materials have $AAE > 1.6$.[17] Although this study covers a small parameter space of the possible aerosol combination of BC core diameters, core-shell ratios and BrC imaginary RI values, the presented data support this classification.

ASSOCIATED CONTENT

Additional information regarding drop cast TEM images from a BC solution, determination of the refractive index of BC and BrC at λ = 660 nm using a cavity ring-down spectrometer, the mass-mobility scaling relationship of BC and HA, the modeling parameters used T-matrix calculations, a comparison of Mie theory and T-matrix calculations for homogeneous and coated spheres, a comparison of BC MAC from Figure 2b and 2c, TEM images of particle melting and the influence of core/shell size and refractive index on absorption enhancement is provided. This information is available free of charge via the Internet at http://pubs.acs.org/.

Supplementary Material

Refer to Web version on PubMed Central for supplementary material.

References

1. Buseck PR, Adachi K, Andras G, Tompa E, Mihaly P. Ns-Soot: A Material-Based Term for Strongly Light-Absorbing Carbonaceous Particles. Aerosol Sci Technol. 2014; 48(7):777–788.
2. Bond TC, Doherty SJ, Fahey DW, Forster PM, Berntsen T, DeAngelo BJ, Flanner MG, Ghan S, Karcher B, Koch D, Kinne S, Kondo Y, Quinn PK, Sarofim MC, Schultz MG, Schulz M, Venkataraman C, Zhang H, Zhang S, Bellouin N, Guttikunda SK, Hopke PK, Jacobson MZ, Kaiser JW, Klimont Z, Lohmann U, Schwarz JP, Shindell D, Storelvmo T, Warren SG, Zender CS. Bounding the role of black carbon in the climate system: A scientific assessment. J Geophys Res: Atmos. 2013; 118(11):5380–5552.
3. Baynard T, Lovejoy ER, Pettersson A, Brown SS, Lack D, Osthoff H, Massoli P, Ciciora S, Dube WP, Ravishankara AR. Design and Application of a Pulsed Cavity Ring-Down Aerosol Extinction Spectrometer for Field Measurements. Aerosol Sci Technol. 2007; 41(4):447–462.
4. Olfert JS, Symonds JPR, Collings N. The effective density and fractal dimension of particles emitted from a light-duty diesel vehicle with a diesel oxidation catalyst. J Aerosol Sci. 2007; 38(1):69–82.
5. Steiner, DHBaHG. Structure and disposition of particles from a spark ignition engine. Atmos Environ. 1992; 26:997–1003.
6. Reid JS, Hobbs PV, Ferek RJ, Blake DR, Martins JV, Dunlap MR, Liousse C. Physical, chemical, and optical properties of reginal hazes dominated by smoke in Brazil. J Geophys Res. 1998; 103:32059–32080.
7. Fang M, Zheng M, Wang F, To KL, Jaafar AB, Tong SL. The solvent-extractable organic compounds in the Indoesia biomass burning aerosols -- characterzation studies. Atmos Environ. 1999; 33:783–795.
8. China S, Mazzoleni C, Gorkowski K, Aiken AC, Dubey MK. Morphology and mixing state of individual freshly emitted wildfire carbonaceous particles. Nat Commun. 2013:4.
9. Khalizov AF, Xue H, Wang L, Zheng J, Zhang R. Enhanced Light Absorption and Scattering by Carbon Soot Aerosol Internally Mixed with Sulfuric Acid. J Phys Chem A. 2009; 113(6):1066–1074. [PubMed: 19146408]
10. Li J, Anderson JR, Buseck PR. TEM study of aerosol particles from clean and polluted marine boundary layers over the North Atlantic. J Geophys Res: Atmos. 2003; 108(D6)
11. Shiraiwa M, Kondo Y, Moteki N, Takegawa N, Miyazaki Y, Blake DR. Evolution of mixing state of black carbon in polluted air from Tokyo. Geophys Res Lett. 2007; 34(16)
12. Moffet RC, Prather KA. In-situ measurements of the mixing state and optical properties of soot with implications for radiative forcing estimates. Proc Natl Acad Sci USA. 2009; 106(29):11872–11877. [PubMed: 19581581]
13. Adachi K, Buseck PR. Internally mixed soot, sulfates, and organic matter in aerosol particles from Mexico City. Atmos Chem Phys. 2008; 8(21):6469–6481.
14. Bond TC, Habib G, Bergstrom RW. Limitations in the enhancement of visible light absorption due to mixing state. J Geophys Res: Atmos. 2006; 111(D20)
15. Jacobson MZ. Strong radiative heating due to the mixing state of black carbon in atmospheric aerosols. Nature. 2001; 409(6821):695–697. [PubMed: 11217854]
16. Zhang RY, Khalizov AF, Pagels J, Zhang D, Xue HX, McMurry PH. Variability in morphology, hygroscopicity, and optical properties of soot aerosols during atmospheric processing. Proc Natl Acad Sci USA. 2008; 105(30):10291–10296. [PubMed: 18645179]
17. Lack DA, Cappa CD. Impact of brown and clear carbon on light absorption enhancement, single scatter albedo and absorption wavelength dependence of black carbon. Atmos Chem Phys. 2010; 10(9):4207–4220.
18. Yablonovitch E. Statistical ray optics. J Opt Soc Am. 1982; 72(7):899–907.
19. Bond TC, Bergstrom RW. Light absorption by carbonaceous particles: An investigative review. Aerosol Sci Technol. 2006; 40(1):27–67.
20. Lack DA, Cappa CD, Cross ES, Massoli P, Ahern AT, Davidovits P, Onasch TB. Absorption Enhancement of Coated Absorbing Aerosols: Validation of the Photo-Acoustic Technique for Measuring the Enhancement. Aerosol Sci Technol. 2009; 43(10):1006–1012.

21. Cappa CD, Onasch TB, Massoli P, Worsnop DR, Bates TS, Cross ES, Davidovits P, Hakala J, Hayden KL, Jobson BT, Kolesar KR, Lack DA, Lerner BM, Li SM, Mellon D, Nuaaman I, Olfert JS, Petaja T, Quinn PK, Song C, Subramanian R, Williams EJ, Zaveri RA. Radiative Absorption Enhancements Due to the Mixing State of Atmospheric Black Carbon. Science. 2012; 337(6098): 1078–1081. [PubMed: 22936774]
22. Schwarz JP, Spackman JR, Fahey DW, Gao RS, Lohmann U, Stier P, Watts LA, Thomson DS, Lack DA, Pfister L, Mahoney MJ, Baumgardner D, Wilson JC, Reeves JM. Coatings and their enhancement of black carbon light absorption in the tropical atmosphere. J Geophys Res: Atmos. 2008; 113(D3)
23. Lan ZJ, Huang XF, Yu KY, Sun TL, Zeng LW, Hu M. Light absorption of black carbon aerosol and its enhancement by mixing state in an urban atmosphere in South China. Atmos Environ. 2013; 69:118–123.
24. Nakayama T, Ikeda Y, Sawada Y, Setoguchi Y, Ogawa S, Kawana K, Mochida M, Ikemori F, Matsumoto K, Matsumi Y. Properties of light-absorbing aerosols in the Nagoya urban area, Japan, in August 2011 and January 2012: Contributions of brown carbon and lensing effect. J Geophys Res: Atmos. 2014; 119(22):12721–12739.
25. Liu S, Aiken AC, Gorkowski K, Dubey MK, Cappa CD, Williams LR, Herndon SC, Massoli P, Fortner EC, Chhabra PS, Brooks WA, Onasch TB, Jayne JT, Worsnop DR, China S, Sharma N, Mazzoleni C, Xu L, Ng NL, Liu D, Allan JD, Lee JD, Fleming ZL, Mohr C, Zotter P, Szidat S, Prevot ASH. Enhanced light absorption by mixed source black and brown carbon particles in UK winter. Nat Commun. 2015:6.
26. Peng J, Hu M, Guo S, Du Z, Zheng J, Shang D, Levy Zamora M, Zeng L, Shao M, Wu Y-S, Zheng J, Wang Y, Glen CR, Collins DR, Molina MJ, Zhang R. Markedly enhanced absorption and direct radiative forcing of black carbon under polluted urban environments. Proc Natl Acad Sci USA. 2016; 113(16):4266–4271. [PubMed: 27035993]
27. Fuller KA, Malm WC, Kreidenweis SM. Effects of mixing on extinction by carbonaceous particles. J Geophys Res: Atmos. 1999; 104(D13):15941–15954.
28. Adachi K, Chung SH, Buseck PR. Shapes of soot aerosol particles and implications for their effects on climate. J Geophys Res: Atmos. 2010:115.
29. Mackowski DW. A simplified model to predict the effects of aggregation on the absorption properties of soot particles. J Quant Spectrosc Radiat Transfer. 2006; 100(1–3):237–249.
30. Scarnato BV, Vahidinia S, Richard DT, Kirchstetter TW. Effects of internal mixing and aggregate morphology on optical properties of black carbon using a discrete dipole approximation model. Atmos Chem Phys. 2013; 13(10):5089–5101.
31. Schnaiter M, Linke C, Mohler O, Naumann KH, Saathoff H, Wagner R, Schurath U, Wehner B. Absorption amplification of black carbon internally mixed with secondary organic aerosol. J Geophys Res: Atmos. 2005; 110(D19)
32. Shiraiwa M, Kondo Y, Iwamoto T, Kita K. Amplification of Light Absorption of Black Carbon by Organic Coating. Aerosol Sci Technol. 2010; 44(1):46–54.
33. Cross ES, Onasch TB, Ahern A, Wrobel W, Slowik JG, Olfert J, Lack DA, Massoli P, Cappa CD, Schwarz JP, Spackman JR, Fahey DW, Sedlacek A, Trimborn A, Jayne JT, Freedman A, Williams LR, Ng NL, Mazzoleni C, Dubey M, Brem B, Kok G, Subramanian R, Freitag S, Clarke A, Thornhill D, Marr LC, Kolb CE, Worsnop DR, Davidovits P. Soot Particle Studies—Instrument Inter-Comparison—Project Overview. Aerosol Sci Technol. 2010; 44(8):592–611.
34. Schnaiter M, Horvath H, Mohler O, Naumann KH, Saathoff H, Schock OW. UV-VIS-NIR spectral optical properties of soot and soot-containing aerosols. J Aerosol Sci. 2003; 34(10):1421–1444.
35. Thompson JE, Hayes PL, Jimenez JL, Adachi K, Zhang XL, Liu JM, Weber RJ, Buseck PR. Aerosol optical properties at Pasadena, CA during CalNex 2010. Atmos Environ. 2012; 55:190–200.
36. Jacobson MZ. Comment on “Radiative Absorption Enhancements Due to the Mixing State of Atmospheric Black Carbon”. Science. 2013; 339(6118)
37. Moosmüller H, Chakrabarty RK, Arnott WP. Aerosol light absorption and its measurement: A review. J Quant Spectrosc Radiat Transfer. 2009; 110(11):844–878.

38. Russell PB, Bergstrom RW, Shinozuka Y, Clarke AD, DeCarlo PF, Jimenez JL, Livingston JM, Redemann J, Dubovik O, Strawa A. Absorption Angstrom Exponent in AERONET and related data as an indicator of aerosol composition. Atmos Chem Phys. 2010; 10(3):1155–1169.
39. Bahadur R, Praveen PS, Xu YY, Ramanathan V. Solar absorption by elemental and brown carbon determined from spectral observations. Proc Natl Acad Sci USA. 2012; 109(43):17366–17371. [PubMed: 23045698]
40. Kirchstetter TW, Novakov T, Hobbs PV. Evidence that the spectral dependence of light absorption by aerosols is affected by organic carbon. J Geophys Res: Atmos. 2004; 109(D21)
41. Yang M, Howell SG, Zhuang J, Huebert BJ. Attribution of aerosol light absorption to black carbon, brown carbon, and dust in China - interpretations of atmospheric measurements during EAST-AIRE. Atmos Chem Phys. 2009; 9(6):2035–2050.
42. Bergstrom RW, Pilewskie P, Russell PB, Redemann J, Bond TC, Quinn PK, Sierau B. Spectral absorption properties of atmospheric aerosols. Atmos Chem Phys. 2007; 7(23):5937–5943.
43. Sandradewi J, Prevot ASH, Szidat S, Perron N, Alfarra MR, Lanz VA, Weingartner E, Baltensperger U. Using aerosol light absorption measurements for the quantitative determination of wood burning and traffic emission contributions to particulate matter. Environ Sci Technol. 2008; 42(9):3316–3323. [PubMed: 18522112]
44. Levin EJT, McMeeking GR, Carrico CM, Mack LE, Kreidenweis SM, Wold CE, Moosmuller H, Arnott WP, Hao WM, Collett JL, Malm WC. Biomass burning smoke aerosol properties measured during Fire Laboratory at Missoula Experiments (FLAME). J Geophys Res: Atmos. 2010:115.
45. Clarke A, McNaughton C, Kapustin V, Shinozuka Y, Howell S, Dibb J, Zhou J, Anderson B, Brekhovskikh V, Turner H, Pinkerton M. Biomass burning and pollution aerosol over North America: Organic components and their influence on spectral optical properties and humidification response. J Geophys Res: Atmos. 2007; 112(D12)
46. Haisch C, Menzenbach P, Bladt H, Niessner R. A Wide Spectral Range Photoacoustic Aerosol Absorption Spectrometer. Anal Chem. 2012; 84(21):8941–8945. [PubMed: 23035870]
47. Wiegand JR, Mathews LD, Smith GD. A UV–Vis Photoacoustic Spectrophotometer. Anal Chem. 2014; 86(12):6049– 6056. [PubMed: 24905953]
48. Radney JG, Zangmeister CD. Measurement of Gas and Aerosol Phase Absorption Spectra across the Visible and Near-IR Using Supercontinuum Photoacoustic Spectroscopy. Anal Chem. 2015; 87:7356. [PubMed: 26098142]
49. Sharma N, Arnold IJ, Moosmüller H, Arnott WP, Mazzoleni C. Photoacoustic and nephelometric spectroscopy of aerosol optical properties with a supercontinuum light source. Atmos Meas Tech. 2013; 6(12):3501–3513.
50. Moosmüller H, Chakrabarty RK, Ehlers KM, Arnott WP. Absorption Ångström coefficient, brown carbon, and aerosols: basic concepts, bulk matter, and spherical particles. Atmos Chem Phys. 2011; 11(3):1217–1225.
51. Moosmüller H, Engelbrecht JP, Skiba M, Frey G, Chakrabarty RK, Arnott WP. Single scattering albedo of fine mineral dust aerosols controlled by iron concentration. J Geophys Res: Atmos. 2012; 117(D11):D11210.
52. Lewis K, Arnott WP, Moosmüller H, Wold CE. Strong spectral variation of biomass smoke light absorption and single scattering albedo observed with a novel dual-wavelength photoacoustic instrument. J Geophys Res: Atmos. 2008; 113(D16):D16203.
53. Gyawali M, Arnott WP, Lewis K, Moosmüller H. In situ aerosol optics in Reno, NV, USA during and after the summer 2008 California wildfires and the influence of absorbing and non-absorbing organic coatings on spectral light absorption. Atmos Chem Phys. 2009; 9(20):8007–8015.
54. Radney JG, Zangmeister CD. Practical limitations of aerosol separation by a tandem differential mobility analyzer–aerosol particle mass analyzer. Aerosol Sci Technol. 2016; 50(2):160–172. [PubMed: 28663667]
55. Hunt GR. Infrared spectral behavior of fine particulate solids. J Phys Chem. 1976; 80(11):1195–1198.
56. Khalizov AF, Lin Y, Qiu C, Guo S, Collins D, Zhang R. Role of OH-Initiated Oxidation of Isoprene in Aging of Combustion Soot. Environ Sci Technol. 2013; 47(5):2254–2263. [PubMed: 23379649]

57. China S, Scarnato B, Owen RC, Zhang B, Ampadu MT, Kumar S, Dzepina K, Dziobak MP, Fialho P, Perlinger JA, Hueber J, Helmig D, Mazzoleni LR, Mazzoleni C. Morphology and mixing state of aged soot particles at a remote marine free troposphere site: Implications for optical properties. Geophys Res Lett. 2015; 42(4):1243–1250.
58. Kozlov VS, Panchenko MV, Tikhomirov AB, Tikhomirov BA, Shmargunov VP. Effect of relative air humidity on photoacoustic aerosol absorption measurements in the near-ground atmospheric layer. Atmos Oceanic Opt. 2011; 24(5):487–491.
59. Langridge JM, Richardson MS, Lack DA, Brock CA, Murphy DM. Limitations of the Photoacoustic Technique for Aerosol Absorption Measurement at High Relative Humidity. Aerosol Sci Technol. 2013; 47(11):1163–1173.
60. Lewis KA, Arnott WP, Moosmüller H, Chakrabarty RK, Carrico CM, Kreidenweis SM, Day DE, Malm WC, Laskin A, Jimenez JL, Ulbrich IM, Huffman JA, Onasch TB, Trimborn A, Liu L, Mishchenko MI. Reduction in biomass burning aerosol light absorption upon humidification: roles of inorganically-induced hygroscopicity, particle collapse, and photoacoustic heat and mass transfer. Atmos Chem Phys. 2009; 9(22):8949–8966.
61. Murphy DM. The Effect of Water Evaporation on Photoacoustic Signals in Transition and Molecular Flow. Aerosol Sci Technol. 2009; 43(4):356–363.
62. Havey DK, Bueno PA, Gillis KA, Hodges JT, Mulholland GW, van Zee RD, Zachariah MR. Photoacoustic Spectrometer with a Calculable Cell Constant for Measurements of Gases and Aerosols. Anal Chem. 2010; 82(19):7935–7942. [PubMed: 20804170]
63. Mackowski, DW. MSTM: A Multiple Sphere T-Matrix FORTRAN Code for Use on Parallel Computer Clusters, version 3.0. National Aeronautics and Space Administration; New York: Goddard Institute for Space Studies; 2013.
64. Witten TA, Sander LM. Diffusion-Limited Aggregation, a Kinetic Critical Phenomenon. Phys Rev Lett. 1981; 47(19):1400–1403.
65. Radney JG, You R, Ma X, Conny JM, Zachariah MR, Hodges JT, Zangmeister CD. Dependence of soot optical properties on particle morphology: measurements and model comparisons. Environ Sci Technol. 2014; 48(6):3169–76. [PubMed: 24548253]
66. Clarke AD, Shinozuka Y, Kapustin VN, Howell S, Huebert B, Doherty S, Anderson T, Covert D, Anderson J, Hua X, Moore KG, McNaughton C, Carmichael G, Weber R. Size distributions and mixtures of dust and black carbon aerosol in Asian outflow: Physiochemistry and optical properties. J Geophys Res: Atmos. 2004; 109(D15)
67. Janzen J. The Refractive Index of Carbon Black. J Colloid Interface Sci. 1979; 69:436–447.
68. Chang H, Charalampopoulos TT. Determination of the Wave-length Dependence of Refractive Indices of Flame Soot. Proc R Soc Lond A. 1990; 430:577–591.
69. Marley NA, Gaffney JS, Baird JC, Blazer CA, Drayton PJ, Frederick JE. An Empirical Method for the Determination of the Complex Refractive Index of Size-Fractionated Atmospheric Aerosols for Radiative Transfer Calculations. Aerosol Sci Technol. 2001; 34:535–549.
70. Knox A, Evans GJ, Brook JR, Yao X, Jeong CH, Godri KJ, Sabaliauskas K, Slowik JG. Mass Absorption Cross-Section of Ambient Black Carbon Aerosol in Relation to Chemical Age. Aerosol Sci Technol. 2009; 43(6):522–532.
71. Feng Y, Ramanathan V, Kotamarthi VR. Brown carbon: a significant atmospheric absorber of solar radiation? Atmos Chem Phys. 2013; 13(17):8607–8621.

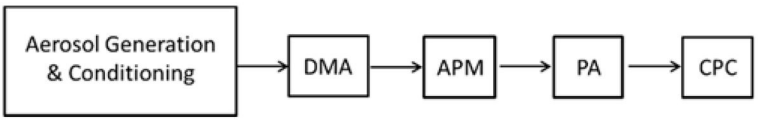

Figure 1.

Experimental schematic used for the characterization of aerosol size, mass and optical absorption properties. Abbreviations: differential mobility analyzer (DMA), aerosol particle mass analyzer (APM), photoacoustic spectrometer (PA) and condensation particle counter (CPC).

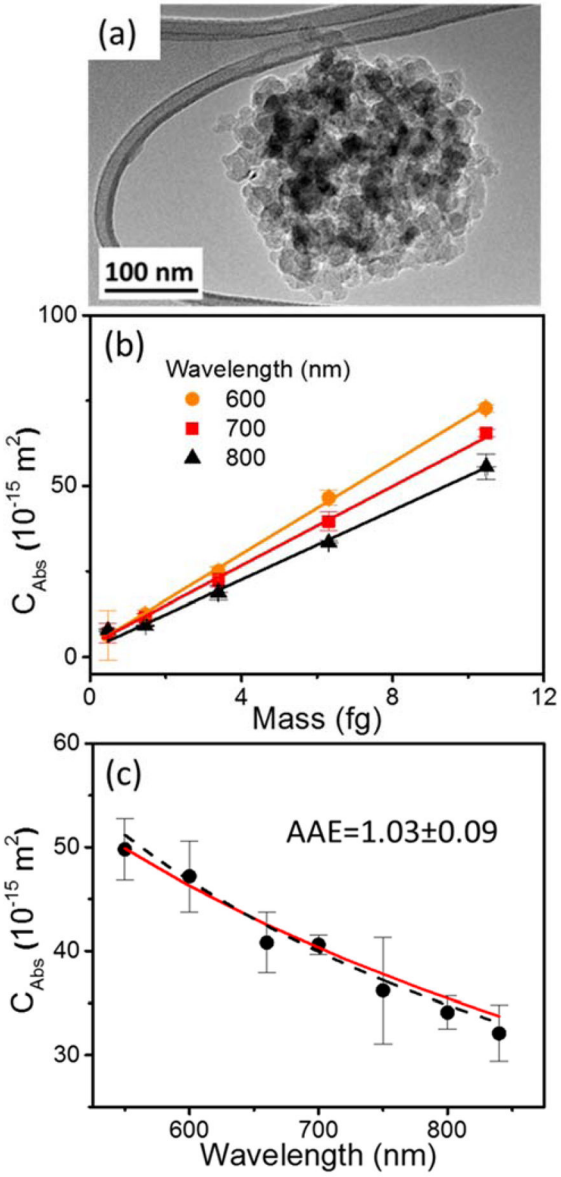

Figure 2.

a) TEM image of bare 250 nm BC particles used in study. b) BC absorption cross section (C_{Abs}) as a function of particle mass at λ = 600 nm, 700 nm and 800 nm. c) Absorption spectrum (C_{Abs}) of 250 nm BC from λ = 550 nm to 840 nm. Dashed black line represents *AAE* fit of the experimental data over full range. Solid red line represents calculated absorption spectrum utilizing T-matrix method described in text. Measured results are reported as experimental mean and 2σ uncertainty propagated across all measurements.

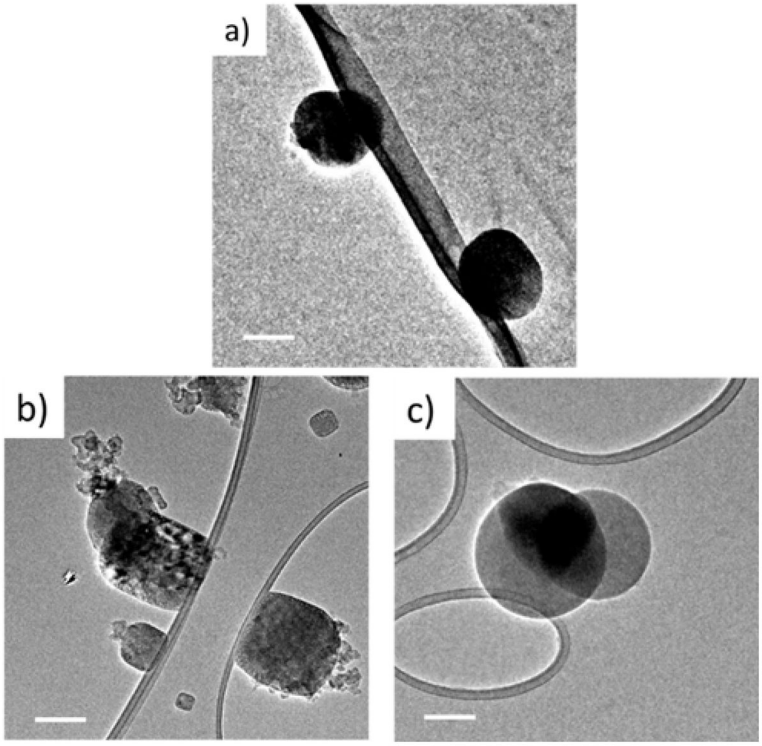

Figure 3.
TEM images of 250 nm a) AS/BC, b) NaCl/BC, c) HA/BC. The scale bar corresponds to 100 nm.

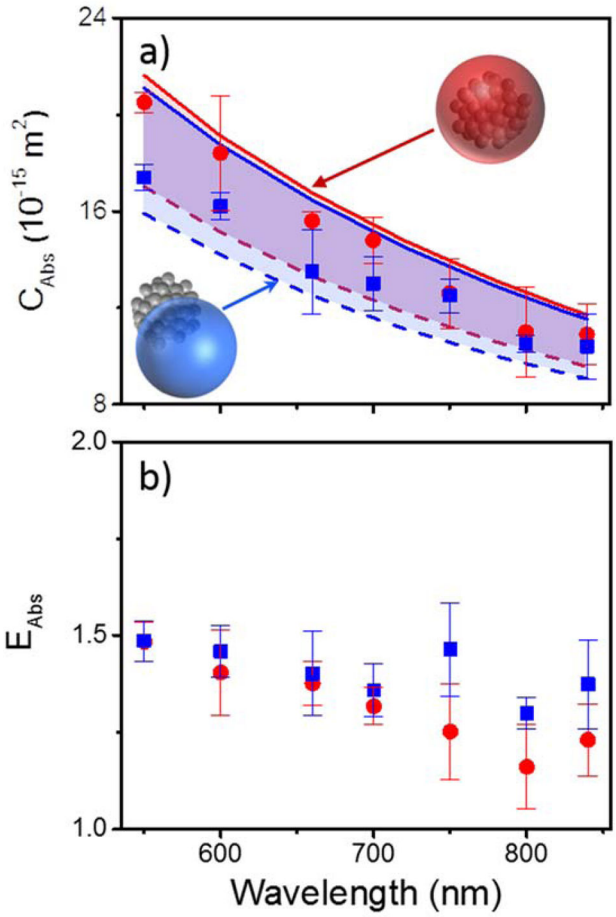

Figure 4.

a) Measured absorption cross section (C_{Abs}) spectra of AS/BC (red circles) and NaCl/BC (blue squares) for 250 nm mass selected particles (χ_{BC} = 0.13) from λ = 550 nm to 840 nm. Lines represent fully embedded (solid) and half embedded (dashed) BC for each system; the shaded regions represent mixing states in between these two extremes. b) E_{Abs} for AS/BC (red circles) and NaCl/BC (blue squares). Measured results are reported as experimental mean and 2σ uncertainty propagated across all measurements.

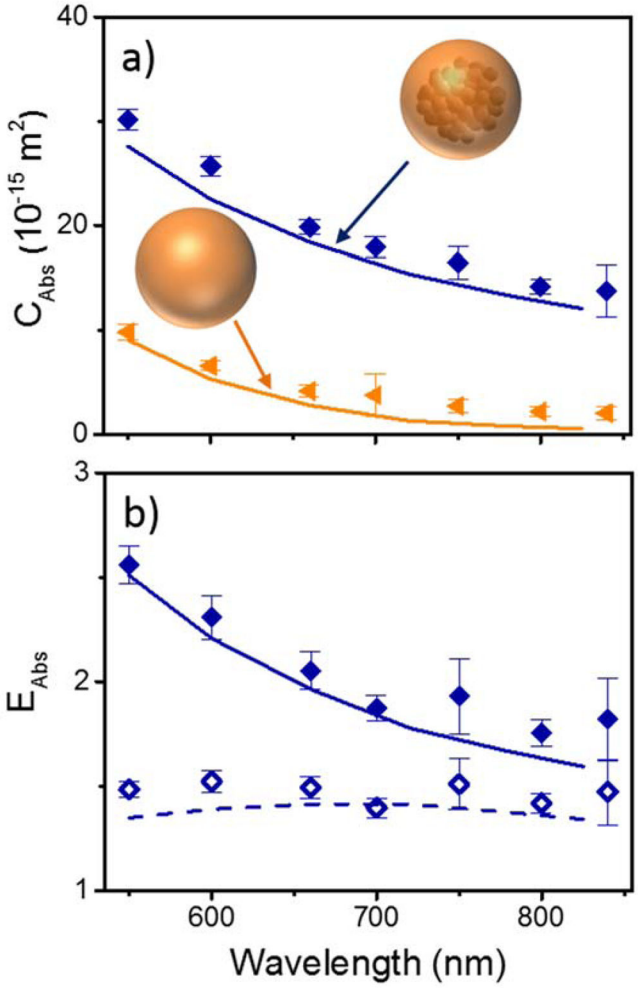

Figure 5.

a) Measured absorption cross section (C_{Abs}) spectra of pure HA (gold triangles) and HA/BC (blue diamonds) with χ_{BC} = 0.13 for 250 nm size-mass selected particles from λ = 550 nm to 840 nm. Lines represent calculated C_{Abs} for each system. b) E_{Abs} for HA/BC including HA absorption (solid blue diamonds) and only including enhancement from HA after subtraction HA absorption (open blue diamonds); see Eq. 8 in discussion and text. Lines represent calculated E_{Abs} using fully internal mixing model for both definitions. Measured results are reported as experimental mean and 2σ uncertainty propagated across all measurements.

Table 1

Measured and modeled *AAE*s for half- and fully-embedded AS/BC and NaCl/BC. Propagated uncertainties are shown along with the fit *AAE*s.

	Measured *AAE*	Calculated *AAE*	
		half-embedded	fully-embedded
AS/BC	1.43 ± 0.05	1.36	1.45
NaCl/BC	1.34 ± 0.06	1.32	1.41